Supporting Information

Proton-Coupled Charge Transfer Inducing Magnetic Phase Transition in Layered Metal-Organic Frameworks

Ke Ji,[a,b] Chisa Itoh, [a,b] Ryota Nasu,[c] Kaito Taka,[c] Ren Inoue,[c] Wataru Kosaka,[a,b] Haruka Yoshino,[a,b] Yasutaka Kitagawa,[c] and Hitoshi Miyasaka*[a,b]

[a] Institute for Materials Research, Tohoku University, 2-1-1 Katahira, Aoba-ku, Sendai 980-8577, Japan.

[b] Department of Chemistry, Graduate School of Science, Tohoku University, 6-3 Aramaki-Aza-Aoba, Aoba-ku, Sendai 980-8578, Japan

[c] Department of Materials Engineering Science, Graduate School of Engineering Science, The University of Osaka, 1-3 Machikaneyama, Toyonaka, Osaka 560-8531, Japan

Corresponding author*

Prof. Dr. Hitoshi Miyasaka

Institute for Materials Research

Tohoku University

2–1–1 Katahira, Aoba-ku, Sendai 980-8577, Japan

E-mail: hitoshi.miyasaka.e7@tohoku.ac.jp

Tel: +81-22-215-2030

FAX: +81-22-215-2031

■ Contents for SI

Table S1. Relevant HOMO energy (eV) and relative angels $\Delta\theta$ (°) of $[Ru_2(4\text{-F-2-OHArCO}_2)_4(THF)_2]$, where $\Delta\theta$ is defined by the angle formed between the plane defined by C_{Ar}–C_{Ar}–O atoms and the plane defined by C_{Ar}–O–H atoms in Ar–O–H group. Since the homoleptic complex contains two independent benzoate ligands, in the "both" condition, the $\Delta\theta$ value for both benzoate ligands is changed simultaneously, while in the "Bz1" and "Bz2" conditions, the $\Delta\theta$ value is changed only for one of the benzoate ligands.

$\Delta\theta$/ °	HOMO energy / eV		
	Bz1	Bz2	Both
0	−4.99220	−4.99220	−4.99220
30	−4.92717	−4.90622	−4.84118
60	−4.79111	−4.76499	−4.56417
90	−4.65859	−4.63628	−4.30403
120	−4.56199	−4.55002	−4.12171
150	−4.51192	−4.50947	−4.03110
180	−4.49396	−4.50022	−4.00334
210	−4.50784	−4.52390	−4.04117
240	−4.55138	−4.57968	−4.14049
270	−4.64090	−4.68036	−4.32961
300	−4.77152	−4.81098	−4.59029
330	−4.91411	−4.94050	−4.86241
360	−4.99220	−4.99220	−4.99220

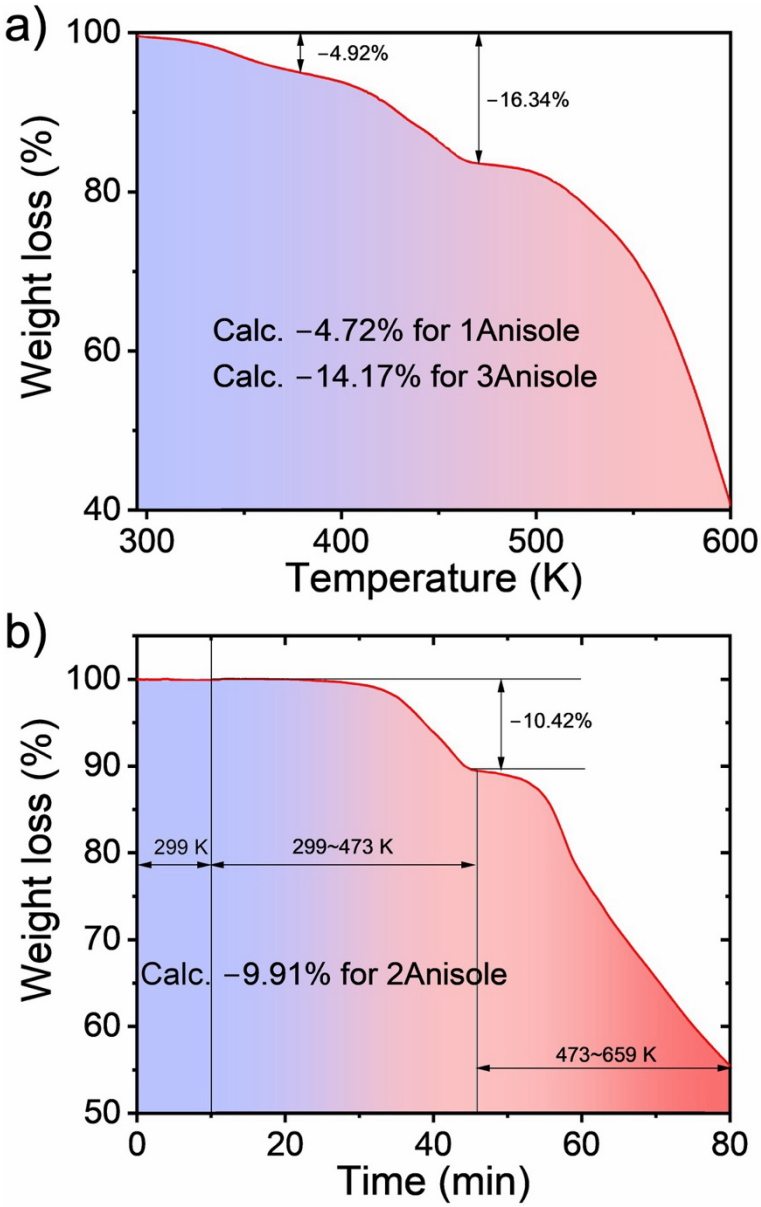

Figure S1. (a) TGA profiles of **1-3Ani** with a heating rate of 5 K min^{-1}. (a) TGA profiles of **1-2Ani** with a temperature of 299 K maintained for 10 minutes, followed by heating initiation at a rate of 5 K min^{-1}.

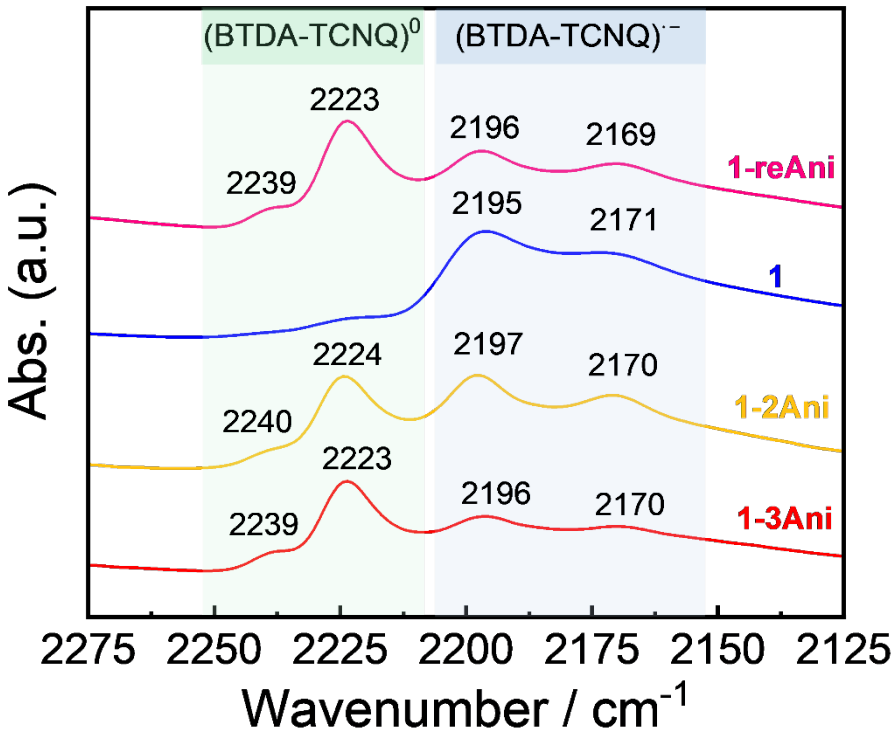

Figure S2. Infrared (IR) spectra of **1-3Ani** (red), **1-2Ani** (orange), **1** (blue), and **1-reAni** (pink) in the C≡N stretching region.

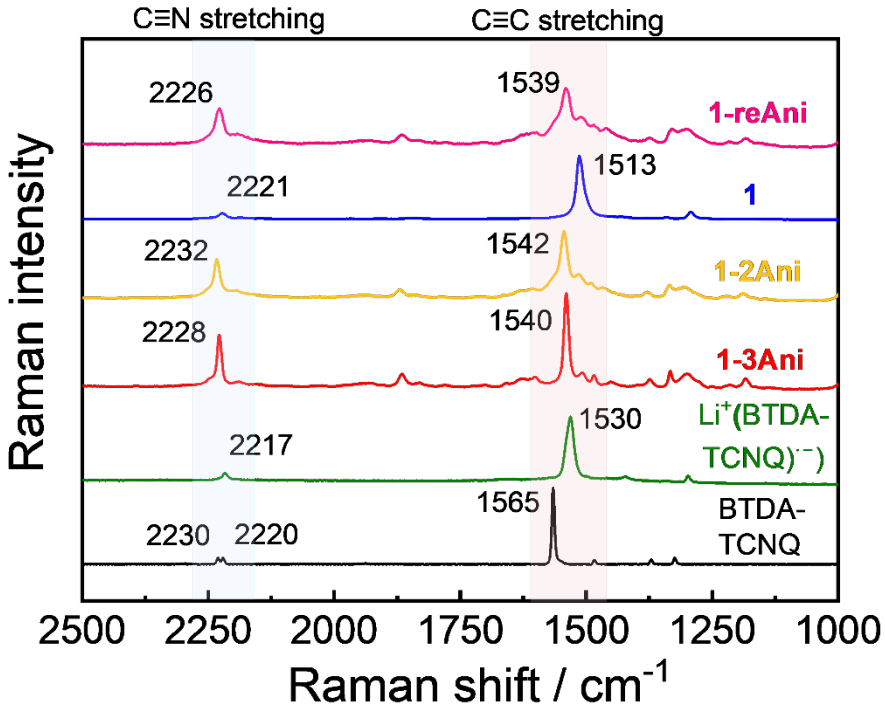

Figure S3. Raman spectra of the original neutral BTDA-TCNQ (black), $Li^{+}(BTDA\text{-}TCNQ)^{\cdot-}$ (green), **1-3Ani** (red), **1-2Ani** (orange), **1** (blue), and **1-reAni** (pink) in the wavenumber range of 2500−1000 cm^{-1}.

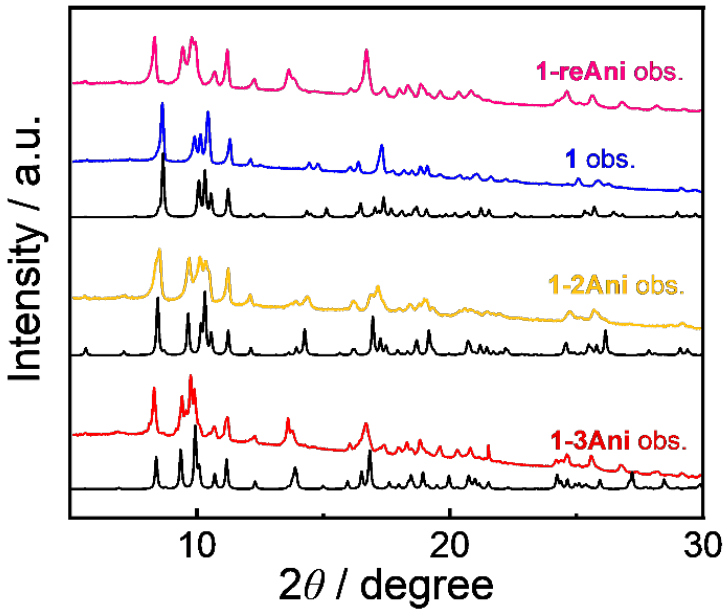

Figure S4. Experimental (color) and simulated (black) PXRD pattern of **1-3Ani** (red), **1-2Ani** (orange), **1** (blue), and **1-reAni** (pink).

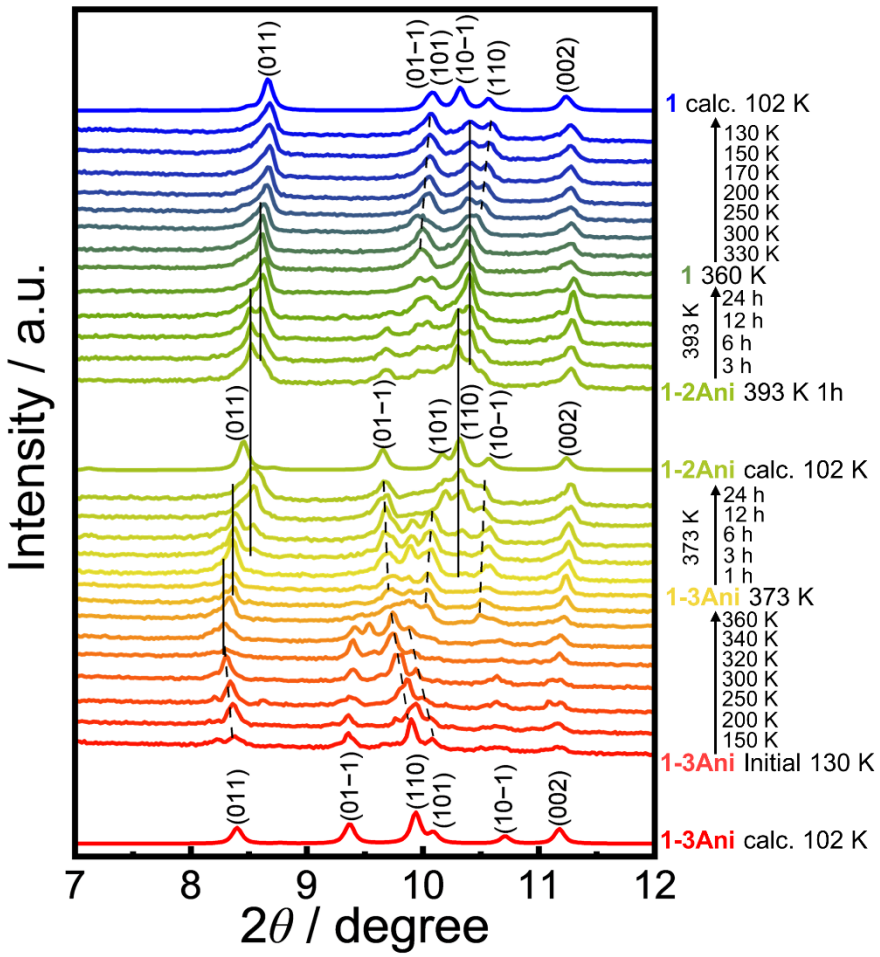

Figure S5. In-suit PXRD pattens for **1-3Ani** during desolvation process. where the fresh sample was evacuated for 24 h at 373 K and then evacuated for 24 h at 393 K. The peak shifts of **1-3Ani** during the heating process and of **1** during the cooling process were also recorded. The **1-3Ani** calc., **1-2Ani** calc., and **1** calc. were simulated patterns obtained from respective single-crystal X-ray crystallography.

Table S2. Crystallographic data for **1-3Ani**, **1-2Ani**, and **1**.

	1-3Ani	**1-2Ani**	**1**	**1-reAni**
Empirical formula	$C_{89}H_{56}F_8N_8O_{27}Ru_4S_2$	$C_{82}H_{48}F_8N_8O_{26}Ru_4S_2$	$C_{68}H_{32}F_8N_8O_{24}Ru_4S_2$	$C_{89}H_{56}F_8N_8O_{27}Ru_4S_2$
Formula weight	2289.81	2181.68	1965.41	2289.81
Temperature / K	102	102	102	102
Crystal system	triclinic	triclinic	triclinic	triclinic
Space group	*P*-1	*P*-1	*P*-1	*P*-1
a / Å	10.3575(5)	10.3301(4)	10.4147(3)	10.4064(5)
b / Å	13.1766(8)	12.6888(4)	11.9786(3)	13.2309(5)
c / Å	15.9839(8)	15.9334(6)	15.8767(4)	16.0151(6)
α / °	82.614(4)	81.582(3)	81.020(2)	82.318(3)
β / °	84.729(4)	86.102(3)	87.138(2)	84.290(4)
γ / °	77.012(4)	80.190(3)	81.835(2)	76.534(3)
Volume / Å^3	2103.5(2)	2033.80(13)	1935.78(9)	2119.84(16)
Z	1	1	1	1
ρ_{calc} / g·cm^3	1.808	1.781	1.686	1.794
μ / mm^{-1}	0.862	0.886	0.918	0.855
F(000)	1142.0	1084.0	968.0	1142.0
Crystal size / mm^3	0.06 × 0.04 × 0.03	0.33 × 0.12 × 0.1	0.32 × 0.28 × 0.06	0.13 × 0.11 × 0.08
Radiation	MoKα (λ = 0.71073)	Mo Kα (λ = 0.71073)	MoKα (λ = 0.71073)	MoKα (λ = 0.71073)
2θ range for data collection / °	3.192 to 57.392	3.288 to 59.476	3.474 to 59.574	3.186 to 60.094
Index ranges	−13 ≤ h ≤ 13, −17 ≤ k ≤ 15, −20 ≤ l ≤ 19	−14 ≤ h ≤ 13, −17 ≤ k ≤ 17, −21 ≤ l ≤ 21	−13 ≤ h ≤ 14, −16 ≤ k ≤ 15, −20 ≤ l ≤ 21	−13 ≤ h ≤ 14, −17 ≤ k ≤ 17, −20 ≤ l ≤ 21
Reflections collected	22279	27813	24456	25106
Independent reflections	8836 [R_{int} = 0.0427]	9705 [R_{int} = 0.0297]	9256 [R_{int} = 0.0301]	10074 [R_{int} = 0.0361]
Data / restraints / parameters	8836 / 0 / 663	9705 / 1 / 602	9256 / 464 / 715	10074/50/662
Goodness-of-fit on F^2	1.083	1.047	1.044	1.042
Final *R* indexes [I>=2σ (I)]	R_1 = 0.0350, wR_2 = 0.0899	R_1 = 0.0331, wR_2 = 0.0813	R_1 = 0.0422, wR_2 = 0.1067	R_1 = 0.0508, wR_2 = 0.1007
Final *R* indexes [all data]	R_1 = 0.0421, wR_2 = 0.0936	R_1 = 0.0433, wR_2 = 0.0866	R_1 = 0.0586, wR_2 = 0.1173	R_1 = 0.0894, wR_2 = 0.1188
CCDC No.	2570565	2570566	2570567	2570568

$R_1 = \sum||F_c| - |F_o|| / \sum|F_o|$; $wR_2 = [\sum w(F_o^2 - F_c^2)^2 / \sum w(F_o^2)^2]^{1/2}$

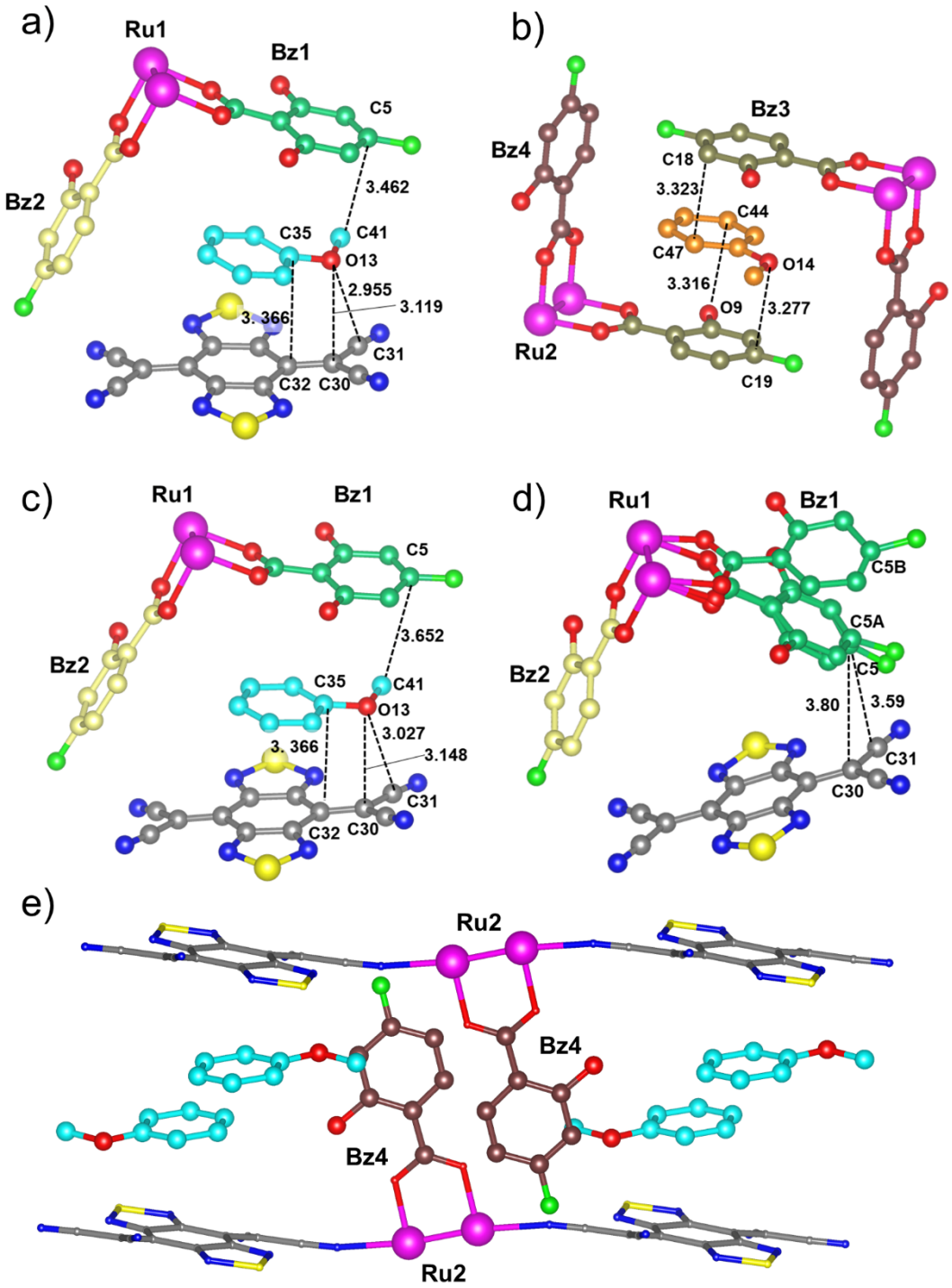

Figure S6. Packing diagrams with anisole molecule coordination mode in **1-3Ani** (a), (b), and **1-2Ani** (c), packing diagram of disorder at Bz1 in **1** after desolvation (d), and coordination environment of Bz4 in **1-3Ani** and **1-2Ani** (e), where the atoms C, O, N, S, F and Ru are represented in gray, red, blue, yellow, green, and pink, respectively. The color of C atoms on Bz1, Bz2, Bz3, Bz4, Ani-1, and Ani-2 are changed to pale green, pale yellow, olive, brown, cyan, and orange respectively, and hydrogen atoms are omitted for clarity.

Table S3. Selected bond distances and angles.

Compound	T / K	[Ru_2] unit	Ru1−Ru1* / Å (Ru2−Ru2*)	Ru1−N1 / Å (Ru2−N2)	Ru1−N1−C29 (Ru2-N2−C31) (δ) / °	Ru-O / Å					
						Ru1−O1 (Ru2−O7)	Ru1−O2 (Ru2−O8)	Ru1−O4 (Ru2−O10)	Ru1−O5 (Ru2−O11)	average	Assignment
1-3Ani	102	Ru1	2.2810(5)[a]	2.360(3)	158.9(2)	2.069(2)	2.058(2)[a]	2.068(2)	2.058(2)[a]	2.0633(10)	$[Ru_2^{II,II}]$
		Ru2	2.2750(4)[b]	2.293(2)	170.3(2)	2.057(2)	2.048(2)[b]	2.0605(18)	2.0650(18)[b]	2.0582(9)	$[Ru_2^{II,II}]$
1-2Ani	102	Ru1	2.2833(4)[a]	2.307(2)	160.2(2)	2.0689(19)	2.0590(19)[a]	2.0659(18)	2.0610(19)[a]	2.0638(9)	$[Ru_2^{II,II}]$
		Ru2	2.2802(4)[b]	2.294(2)	168.4(2)	2.0606(18)	2.0584(18)[b]	2.0566(18)	2.0573(18)[b]	2.0582(9)	$[Ru_2^{II,II}]$
1	102	Ru1	2.2746(5)[c]	2.287(3)	153.8(3)	2.082(6)	2.056(6)[c]	2.052(3)	2.048(3)[c]	2.0538(19)	$[Ru_2^{II,II}]$
		Ru2	2.2782(5)[d]	2.225(3)	173.5(3)	2.018(2)	2.019(2)[d]	2.016(3)	2.019(3)[d]	2.0182(12)	$[Ru_2^{II,III}]^+$
1-reAni	102	Ru1	2.2808(7)[a]	2.358(4)	158.5(3)	2.065(3)	2.058(3)[a]	2.067(3)	2.063(3)[a]	2.0633(15)	$[Ru_2^{II,II}]$
		Ru2	2.2792(7)[b]	2.301(4)	169.6(4)	2.057(3)	2.048(3)[b]	2.066(3)	2.064(3)[b]	2.0588(15)	$[Ru_2^{II,II}]$

*Symmetry code: (a) 1−X, −Y,1−Z; (b) −X,1−Y, −Z; (c) 3−X, −Y,1−Z; (d) 2−X,1−Y, −Z;

Table S4. Bond lengths (Å) on the BTDA-TCNQ moiety and degree of charge transfer (ρ) estimated from the Kistenmacher relationship.[1]

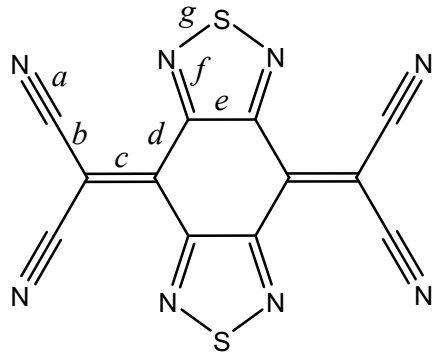

Compound	*a*	*b*	*c*	*d*	*e*	*f*	*g*	ρ^a
BTDA-TCNQ[2]	1.126(5)	1.444(6)	1.351(7)	1.464(6)	1.421(5)	1.330(5)	1.626(4)	0
$[NEt(Me)_3](BTDA\text{-}TCNQ)_3$[3]	1.140(6)	1.429(7)	1.390(6)	1.437(6)	1.433(5)	1.346(6)	1.614(4)	−1
1-3Ani	1.145(4)	1.438(4)	1.381(4)	1.446(4)	1.438(4)	1.331(3)	1.621(3)	−0.65(5)
	1.136(3)	1.436(4)		1.459(4)		1.319(4)	1.607(2)	
1-2Ani	1.140(3)	1.436(3)	1.375(3)	1.457(3)	1.424(3)	1.335(3)	1.622(2)	−0.50(4)
	1.145(3)	1.433(3)		1.463(3)		1.334(3)	1.615(2)	
1	1.146(5)	1.417(5)	1.403(5)	1.429(5)	1.444(5)	1.339(5)	1.612(4)	−1.40(7)
	1.143(4)	1.413(4)		1.433(5)		1.331(5)	1.602(4)	
1-reAni	1.142(5)	1.440(6)	1.382(6)	1.450(5)	1.427(6)	1.327(5)	1.627(4)	−0.65(8)
	1.141(5)	1.436(6)		1.459(6)		1.325(5)	1.617(4)	

[a]Estimated from the Kistenmacher relationship using averaged bond lengths: $\rho = A_H[c/(b + d)] + B_H$, with $A_H = -50.00$ and $B_H = 23.25$.

Table S5. Selected angle (°) and intra-molecular hydrogen bond distances (Å).

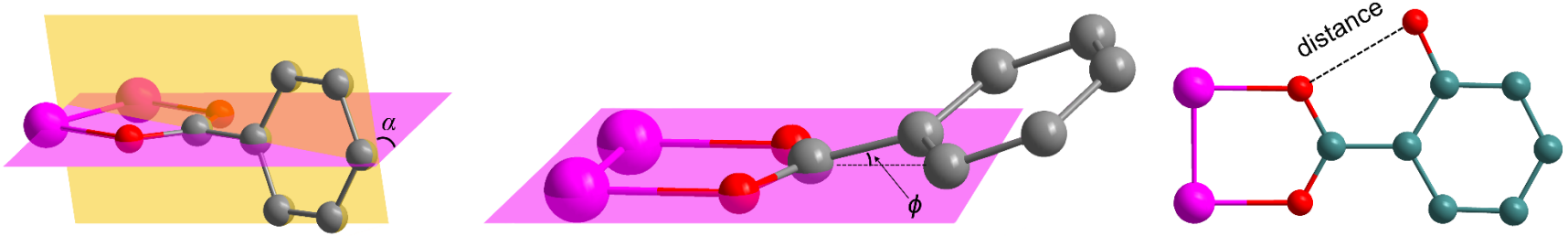

Comp.	T / K	[Ru] unit	α / ° [a]		ϕ / ° [b]		O–H···O* / Å [c]		O–H···O* angle / ° [d]	
			Bz1 (Bz3)	Bz2 (Bz4)	Bz1 (Bz3)	Bz2 (Bz4)	O1–O3 (O7–O9)	O4–O6 (O10–O12)	O1···H3–O3 (O7···H9–O9)	O4···H6–O6 (O10···H12–O12)
1-3Ani	102	Ru1	15.86(8)	1.17(9)	7.82(18)	2.33(18)	2.650(3)	2.582(3)	142.44(19)	150(4)
		Ru2	1.78(8)	8.69(8)	1.57(17)	1.5(2)	2.535(3)	2.558(3)	145.25(16)	144.56(14)
1-2Ani	102	Ru1	23.51(9)	4.99(9)	13.35(19)	5.80(19)	2.660(3)	2.581(3)	141.91(19)	144.67(16)
		Ru2	4.83(11)	12.68(8)	3.19(19)	3.52(18)	2.557(3)	2.550(3)	140.49(18)	138.91(17)
1	102	Ru1	9.0(3)	5.57(14)	0.8(8)	0.7(3)	2.634(9)	2.584(4)	138.4(7)	142.9(2)
		Ru2	6.77(16)	13.48(14)	3.1(3)	5.0(2)	2.594(4)	2.575(7)	143.8(2)	73.6(4)
1-reAni	102	Ru1	15.42(14)	0.91(15)	5.3(3)	1.6(3)	2.656(5)	2.585(5)	142.5(3)	144.9(3)
		Ru2	1.33(15)	8.54(12)	0.2(3)	2.4(3)	2.532(5)	2.555(4)	146.6(3)	145.6(3)

[a] Dihedral angle between the least-squares plane defined by the phenyl ring of benzoate ligand and a carboxylate-bridging mode (atom set of Ru_2O_2C); [b] angel between the C–C bond linking the phenyl ring and the carboxylate-bridging mode in the benzoic acid ligand and the normal to the least-squares plane of the carboxylate-bridging mode (atom set of Ru_2O_2C); [c] distance between the oxygen atom on the *o*-OH group and the oxygen atom of the carboxylate. [d] angle between the oxygen and hydrogen atom on the *o*-OH group and the oxygen atom of the carboxylate.

Table S6. The estimation of the overlap integral.

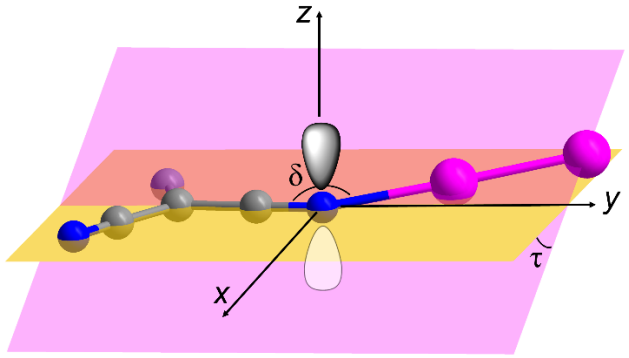

Compound	T / K	[Ru_2] unit	δ / ° [a]	τ / ° [b]	A_σ [c]	A_π [d]
1-3Ani	102	Ru1	158.94	2.79	0.0003	0.9998
		Ru2	170.27	80.22	0.0277	0.9860
1-2Ani	102	Ru1	160.15	11.71	0.0047	0.9976
		Ru2	168.37	70.84	0.0366	0.9815
1	102	Ru1	153.78	20.88	0.0248	0.9875
		Ru2	173.55	58.58	0.0092	0.9954
1-reAni	102	Ru1	158.51	3.54	0.0005	0.9997
		Ru2	169.58	80.69	0.0319	0.9839

[a] ∠Ru-N-C; [b] Dihedral angel between two least-square plane by (Ru−Ru−N≡C−C) and (C−C−(C≡N)$_2$); [c] $A_\sigma = (\sin\delta \sin\tau)^2$; [d] $A_\pi = \{1-(\sin\delta \sin\tau)^2\}^{0.5}$.

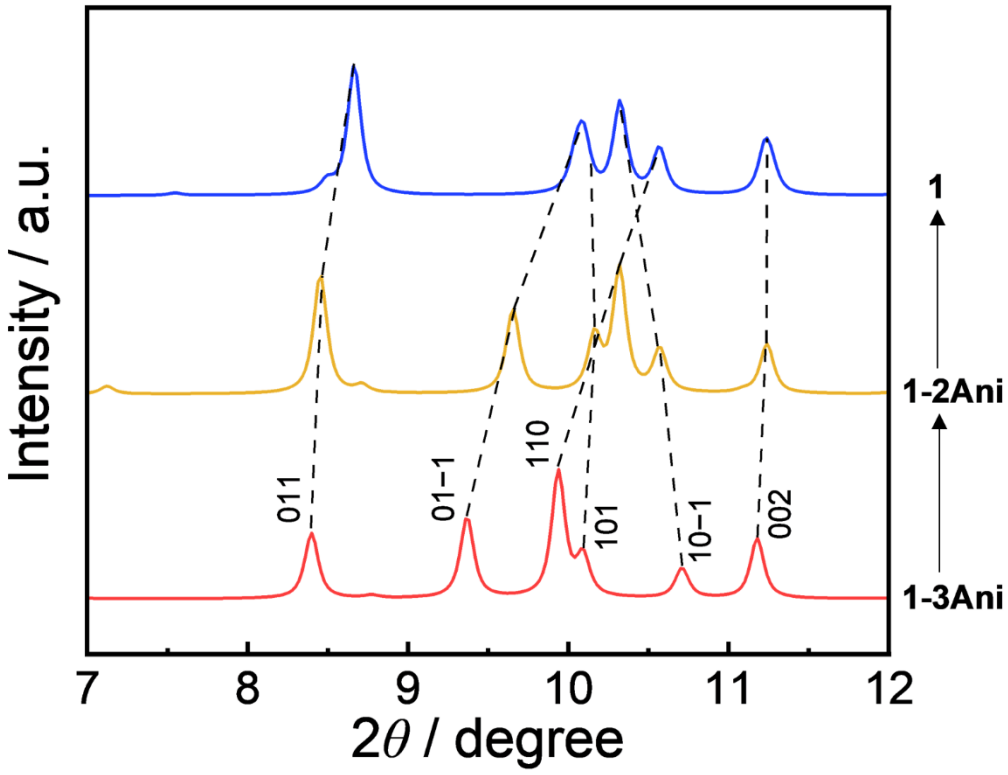

Figure S7. Simulated PXRD pattern of **1-3Ani** (red), **1-2Ani** (orange), and **1** (blue).

Table S7. Summary of the Structural and Magnetic Properties. ψ is the canting angle of [Ru_2] units (D)within the zigzag D_2A layers relative to the ideal flat layer.

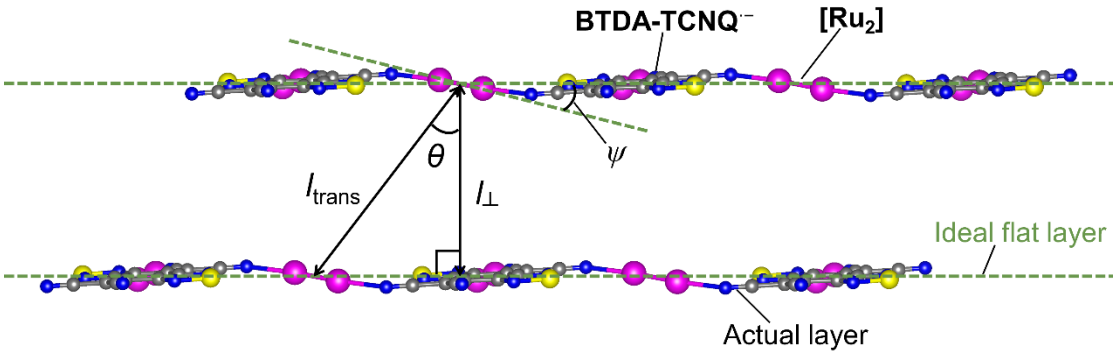

Compound	l_{trans} / Å	l'_{trans} / Å	ψ	Magnetic ground state	Electronic state	Ref.
1-3Ani	10.36	10.41	6.21	PM	N	This work
1-2Ani	10.33	10.40	7.92	PM	N	This work
1	10.41	10.47	7.40	AFM	1e-I	This work
2	10.07	11.21	31.59	PM	2e-I	4
2-PhH	10.04	10.54	22.74	FM	1e-I	4
2-CO_2	10.25	10.78	21.95	FM	1e-I	5
3-CO_2	13.03	13.03	1.03	PM	N	6
3	11.05	11.59	21.47	FM	1e-I	6
4-4DCE	10.70	10.79	8.72	PM	2e-I	7
4-nDCE	10.52	11.03	19.16	FM	1e-I	7

Determination of practical inter-layer translational distance l'_{trans}.
Interlayer dipole interaction (J_{dipole}) could be provided by the following equation:

$$J_{dipole} = \frac{\mu_0}{4\pi}(g\mu_B)^2 \frac{\mu_i\mu_j - 3(\mu_i \cdot \widehat{l_{trans}})(\mu_j \cdot \widehat{l_{trans}})}{l_{trans}^3}$$

where m should be substituted to effective m of $m' = m \cos y$, due to the decrease of magnetic moment parallel to D_2A layer. So, J_{dipole} could be proportional to $\frac{\mu_i\mu_j}{\left(l_{trans}/(cos\psi)^{2/3}\right)^3}$. In this respect we modified

l'_{trans} as $l_{trans}/(\cos\psi)^{2/3}$.

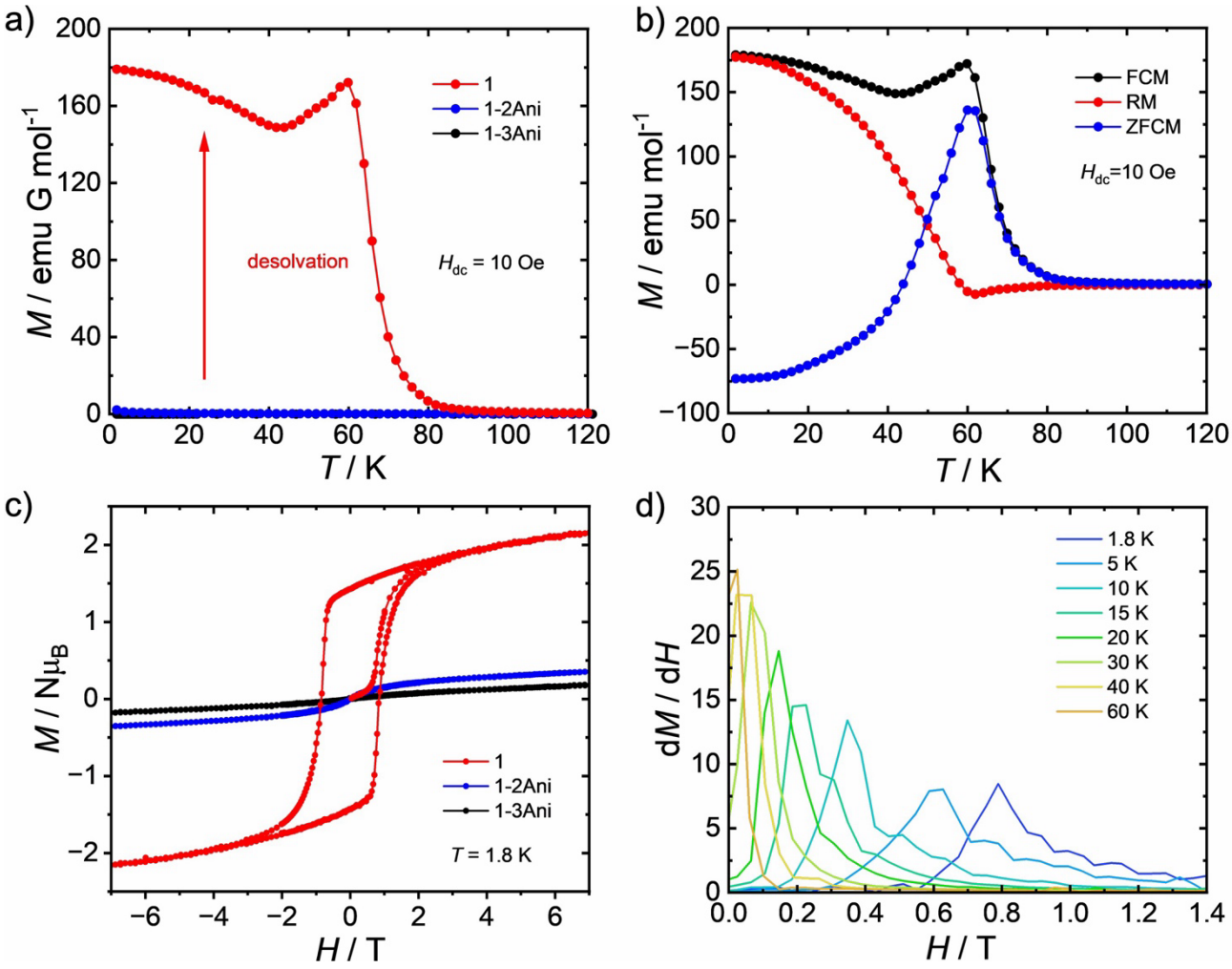

Figure S8. Magnetic properties of **1**. (a) Variation of the magnetization (*M*) in the series (*H* = 10 Oe). (b) Temperature dependence of FCM (black), remnant magnetization (RM, red), and zero-field-cooled magnetization (ZFCM, blue) at 10 Oe. (c) Field dependence of the magnetization for **1-3Ani** (black),**1-2Ani** (blue), and **1** (red) at 1.8 K. (d) d*M*/d*H* vs H plots for the virgin magnetization from *M*-*H* curves.

A coexistence of antiferromagnetic order and spin-glass state is observed below the T_N. In order to study the spin dynamics of **1**, the frequency dependence of the freezing temperature (T_f, corresponding to the cusp temperature in χ''–T plots) was fitted by the critical slowing down model: $\tau = \tau_0(T_f/T_{SG} - 1)^{-zv'}$, where τ ($\tau = 1/f$) is the relaxation time associated with the measured frequency f, τ_0 is the single-flip relaxation time, T_{SG} is the spin glass transition temperature as f tends to 0, and zv' is the dynamic critical exponent.[8,9,10] The value of τ_0 obtained from the best-fit results is 2×10^{-10} s (Figure S11, inset I), which lies within the boundary range between the canonical state (10^{-13}–10^{-12} s) and cluster-glass state (10^{-11}–10^{-4} s).[9,11,12] The zv' value is found to be 6.4, which is in the typical range of spin-glass state formation (4–12). The spin dynamics in glassy systems around the T_f was also simulated by Vogel-Fulcher law, where the frequency dependence can be described as $f = f_0 \exp[-E_a/k_B(T_f - T_0)]$.[9,11] Here f_0 is the characteristic attempt frequency, E_a is the activation energy, and T_0 is the Vogel-Fulcher temperature, which reflects the effective degree of interaction among spins or clusters. From the T_f vs $1/\ln(f_0/f)$ plot (Figure S11, inset II), the fitted value of E_a/k_BT_0 is 1.13, indicating the formation of a cluster-glass-like state in **1** (for typical spin glass systems, this value is usually much smaller than 1, whereas higher values are characteristic of cluster glass systems).[9,11]

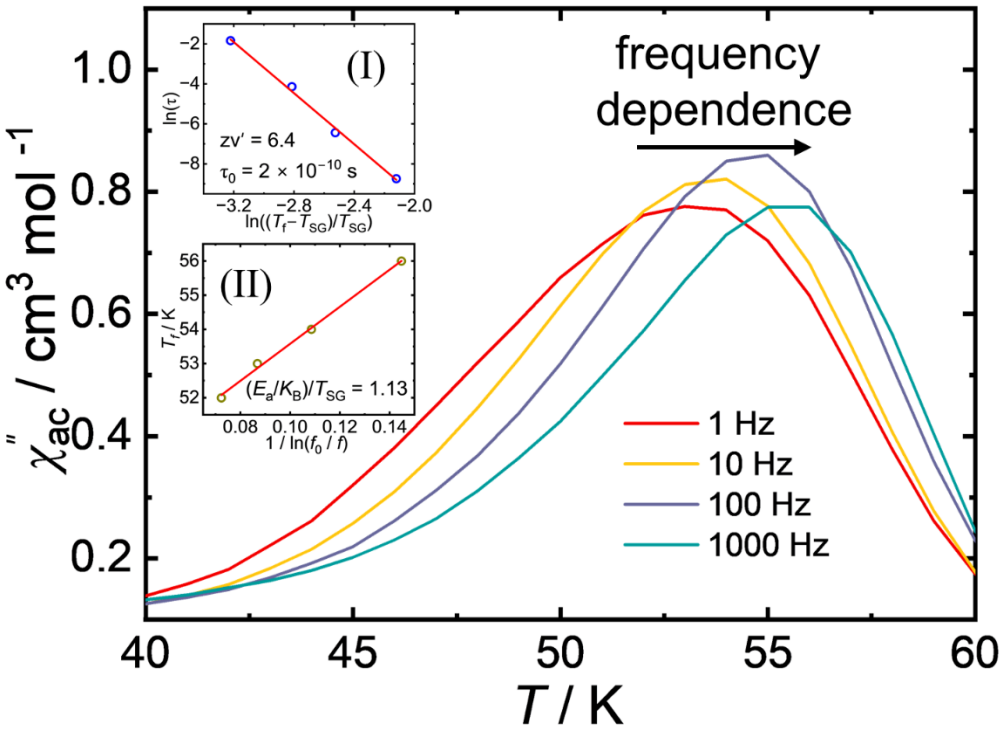

Figure S9. The zoomed view of the frequency dependence in χ″ part for **1**. Inset: (I) The frequency dependence of freezing temperatures plotted as ln(τ) vs $\ln(T_f/T_{SG} - 1)$, where the red line represents the fit to power-law divergence; (II) The frequency dependence of freezing temperatures plotted as T_f vs $1 / \ln(f_0/f)$, where the red line represents the fit to Vogel-Fulcher law.

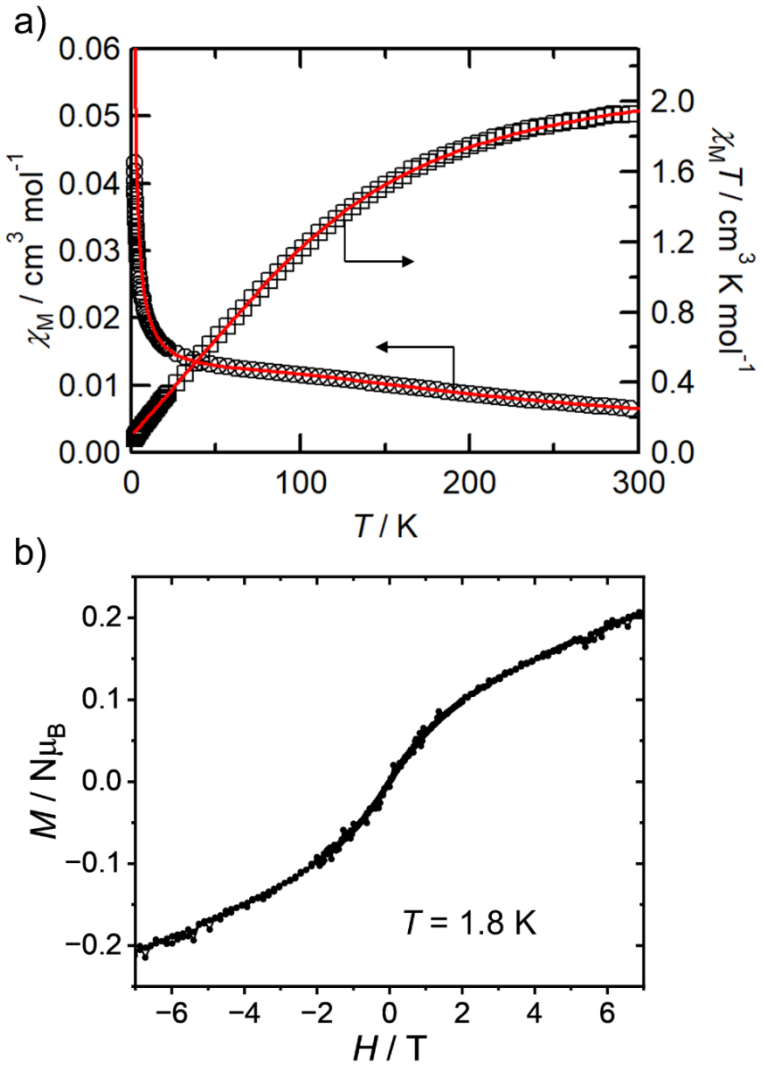

Figure S10. (a) Temperature dependence of χ_M (open circle) and $\chi_M T$ (open square) measured under a DC field of 1000 Oe from 300 to 1.8 K for **1-reAni**. The solid line represents the best-fit line based on a Curie paramagnetic model with $S = 1$ at temperatures ranging from 30 to 300 K, taking into account zero-field splitting (D), temperature-independent term (χ_{TIP}), and impurity with $S = 3/2$ (ρ). The best fitting parameters were: $g = 2.0$ (fixed), $D/k_B = 362.2(13)$ K, $\chi_{TIP} = 116.4(98) \times 10^{-6}$ cm^3 mol^{-1} and $\rho = 0.0252(2)$ for **1-reAni**. (b) Field dependence of the magnetization for **1-reAni** at 1.8 K.

Table S8. Atomic Cartesian coordinates used for DFT calculations of models **1** and **1-3Ani**.

1	Atomic Cartesian coordinates			**1-3Ani**	Atomic Cartesian coordinates		
Atom	*x* / Å	*y* / Å	*z* / Å	Atom	*x* / Å	*y* / Å	*z* / Å
Ru	15.5696	1.9514	7.1170	Ru	5.4240	1.6972	7.2747
Ru	16.4672	0.4384	8.5588	Ru	6.4019	0.0729	8.5429
F	13.2450	-5.1323	3.4346	F	5.2219	-4.6197	1.8924
F	8.8467	0.5495	11.7866	F	-1.1279	-0.2363	12.0481
O	14.8988	0.3875	5.8863	O	4.9381	0.2794	5.8479
O	15.7419	-1.0798	7.3990	O	5.8937	-1.3092	7.1059
O	13.9925	-0.5552	3.6227	O	4.4692	-0.2478	3.2931
H	14.0475	0.0599	4.1917	H	4.5602	0.2673	3.9507
O	13.8004	1.7964	8.1434	O	3.6620	1.3695	8.3077
O	14.6806	0.3109	9.5522	O	4.6302	-0.2257	9.5453
O	11.3995	2.6797	8.5088	O	1.2247	2.0840	8.7671
H	12.1153	2.5895	8.0785	H	2.0701	2.0844	8.4150
C	15.1733	-0.8004	6.3283	C	5.3316	-0.9085	6.0401
C	14.6948	-1.9012	5.4646	C	5.1866	-1.8947	4.9375
C	14.7716	-3.1799	6.0054	C	4.8146	-1.4993	3.6518
H	15.1662	-3.3124	6.8587	C	4.8217	-2.4382	2.6158
C	14.2664	-4.2652	5.2953	H	4.5775	-2.1906	1.7316
H	14.3236	-5.1391	5.6634	C	5.1863	-3.7128	2.9062
C	13.6959	-4.0715	4.0459	C	5.5161	-4.1565	4.1616
C	13.6132	-2.7975	3.5051	H	5.7370	-5.0662	4.3244
H	13.2218	-2.6604	2.6520	C	5.5134	-3.2278	5.1749
C	14.1170	-1.7075	4.2152	H	5.7391	-3.5003	6.0563
C	13.7143	1.0110	9.1437	C	3.6290	0.4925	9.2430
C	12.4155	0.9153	9.8381	C	2.3725	0.3414	9.9921
C	11.3337	1.7280	9.4838	C	1.2364	1.1177	9.7016
C	10.1340	1.6152	10.1595	C	0.0485	0.9180	10.4064
H	9.4008	2.1810	9.9481	H	-0.7218	1.4418	10.2191
C	10.0283	0.6695	11.1345	C	0.0201	-0.0463	11.3697
C	11.0550	-0.1643	11.5217	C	1.1117	-0.8307	11.7034
H	10.9445	-0.8050	12.2144	H	1.0592	-1.4840	12.3910
C	12.2518	-0.0214	10.8492	C	2.2780	-0.6248	10.9959
H	12.9838	-0.5800	11.0846	H	3.0395	-1.1567	11.1975
F	18.7918	7.5221	12.2412	F	6.6039	6.3898	13.9252
F	23.1901	1.8403	3.8892	F	12.9538	2.0063	3.7695
O	17.1380	2.0023	9.7895	O	6.8878	1.4907	9.9697
O	16.2949	3.4696	8.2768	O	5.9322	3.0793	8.7117
O	18.0443	2.9450	12.0531	O	7.3567	2.0178	12.5245
H	17.9893	2.3299	11.4841	H	7.2657	1.5028	11.8668
O	18.2365	0.5934	7.5324	O	8.1639	0.4005	7.5099
O	17.3562	2.0790	6.1236	O	7.1957	1.9957	6.2723
O	20.6373	-0.2899	7.1670	O	10.6012	-0.3139	7.0505
H	19.9215	-0.1997	7.5973	H	9.7557	-0.3143	7.4026
C	16.8635	3.1902	9.3475	C	6.4943	2.6785	9.7775
C	17.3420	4.2910	10.2112	C	6.6393	3.6647	10.8801
C	17.2653	5.5698	9.6704	C	7.0113	3.2693	12.1658
H	16.8706	5.7022	8.8171	C	7.0042	4.2083	13.2018
C	17.7705	6.6550	10.3805	H	7.2484	3.9607	14.0860
H	17.7132	7.5289	10.0124	C	6.6396	5.4829	12.9114
C	18.3409	6.4613	11.6299	C	6.3098	5.9266	11.6560
C	18.4236	5.1873	12.1707	H	6.0889	6.8363	11.4932
H	18.8151	5.0502	13.0238	C	6.3125	4.9979	10.6427
C	17.9198	4.0973	11.4606	H	6.0868	5.2704	9.7613
C	18.3225	1.3788	6.5321	C	8.1968	1.2775	6.5746
C	19.6213	1.4745	5.8377	C	9.4534	1.4287	5.8255
C	20.7032	0.6618	6.1919	C	10.5895	0.6523	6.1160
C	21.9029	0.7746	5.5163	C	11.7774	0.8521	5.4112
H	22.6360	0.2088	5.7277	H	12.5476	0.3283	5.5984
C	22.0085	1.7203	4.5413	C	11.8058	1.8164	4.4479

C	20.9818	2.5542	4.1541	C	10.7142	2.6007	4.1142
H	21.0923	3.1948	3.4614	H	10.7666	3.2541	3.4266
C	19.7850	2.4112	4.8266	C	9.5479	2.3949	4.8217
H	19.0530	2.9698	4.5912	H	8.7864	2.9267	4.6201
Ru	11.6624	5.8581	1.0653	S	1.4188	9.8946	5.7214
Ru	10.8683	5.9990	-1.0653	N	4.2831	3.4064	6.1159
F	10.3663	13.9975	0.7321	N	2.5997	6.0658	3.2167
F	4.0659	3.2511	2.6900	N	1.8345	8.3607	5.3995
O	11.2921	7.8270	1.3119	N	1.4447	9.8422	7.3269
O	10.5157	7.9666	-0.7819	C	2.9216	5.5636	5.7157
O	11.4881	9.9713	2.7574	C	2.5202	6.3996	6.7388
H	11.4883	9.1421	2.6226	C	2.0216	7.7463	6.5654
O	9.7974	5.4262	1.6977	C	1.7786	8.6175	7.6842
O	9.0230	5.5280	-0.3955	C	3.6436	4.3417	5.9495
O	8.1272	5.0787	3.6258	C	2.7385	5.8952	4.3307
H	8.0844	5.9145	3.6943	S	3.0110	4.7150	10.0962
C	10.7995	8.5039	0.3261	N	0.1466	11.2032	9.7017
C	10.6189	9.9397	0.4969	N	1.8301	8.5437	12.6009
C	10.9905	10.5926	1.6914	N	2.5953	6.2489	10.4181
C	10.8771	11.9721	1.7651	N	2.9851	4.7673	8.4907
H	11.1238	12.4404	2.5531	C	0.7862	10.2678	9.8681
C	10.3993	12.6438	0.6647	C	1.5082	9.0460	10.1019
C	9.9855	12.0447	-0.4891	C	1.6913	8.7144	11.4869
H	9.6325	12.5514	-1.2110	C	1.9096	8.2099	9.0788
C	10.1012	10.6815	-0.5643	C	2.4082	6.8632	9.2522
H	9.8245	10.2331	-1.3548	C	2.6512	5.9920	8.1334
C	8.8484	5.2895	0.8481	Ru	1.9453	6.3246	1.0340
C	7.5616	4.8272	1.3230	Ru	1.0161	6.5149	-1.0340
C	7.3169	4.6775	2.6900	F	-0.6779	14.1942	1.6020
C	6.1508	4.1291	3.1602	F	-5.7140	3.7963	3.0170
H	5.9963	4.0098	4.0907	O	1.4381	8.2828	1.4057
C	5.2306	3.7651	2.2354	O	0.5292	8.4626	-0.6272
C	5.3953	3.8790	0.8747	O	1.3881	10.2380	3.0183
H	4.7168	3.5968	0.2725	H	1.6456	9.4978	2.7162
C	6.5777	4.4154	0.4185	O	0.1004	5.7362	1.7382
H	6.7257	4.5059	-0.5160	O	-0.8061	5.8831	-0.2959
F	12.1643	-2.1404	-0.7321	O	-1.3861	5.3694	3.7870
F	18.4647	8.6061	-2.6900	H	-0.6990	5.6237	3.3769
O	11.2386	4.0302	-1.3119	C	0.8201	8.9582	0.4937
O	12.0150	3.8906	0.7819	C	0.4381	10.3322	0.8054
O	11.0425	1.8858	-2.7574	C	0.7329	10.9159	2.0515
H	11.0424	2.7151	-2.6226	C	0.3477	12.2221	2.3189
O	12.7332	6.4310	-1.6977	H	0.5351	12.6218	3.1606
O	13.5077	6.3292	0.3955	C	-0.3116	12.9223	1.3366
O	14.4035	6.7785	-3.6258	C	-0.6090	12.3972	0.0981
H	14.4463	5.9427	-3.6943	H	-1.0620	12.9125	-0.5585
C	11.7311	3.3533	-0.3261	C	-0.2310	11.1046	-0.1518
C	11.9118	1.9174	-0.4969	H	-0.4275	10.7214	-0.9992
C	11.5401	1.2646	-1.6914	C	-0.8983	5.6330	0.9320
C	11.6536	-0.1150	-1.7651	C	-2.1769	5.1879	1.4986
H	11.4068	-0.5833	-2.5531	C	-2.3591	5.0574	2.8908
C	12.1314	-0.7867	-0.6647	C	-3.5568	4.5982	3.3998
C	12.5452	-0.1875	0.4891	H	-3.6800	4.5015	4.3367
H	12.8981	-0.6942	1.2110	C	-4.5652	4.2844	2.5229
C	12.4294	1.1757	0.5643	C	-4.4483	4.4403	1.1509
H	12.7061	1.6240	1.3548	H	-5.1736	4.2386	0.5712
C	13.6822	6.5676	-0.8481	C	-3.2564	4.8923	0.6579
C	14.9691	7.0300	-1.3230	H	-3.1573	5.0083	-0.2798
C	15.2138	7.1797	-2.6900	F	3.6393	-1.3547	-1.6020
C	16.3798	7.7281	-3.1602	F	8.6754	9.0432	-3.0170
H	16.5344	7.8474	-4.0907	O	1.5233	4.5567	-1.4057

C	17.3001	8.0920	-2.2354	O	2.4322	4.3769	0.6272
C	17.1353	7.9781	-0.8747	O	1.5733	2.6015	-3.0183
H	17.8138	8.2604	-0.2725	H	1.3158	3.3417	-2.7162
C	15.9529	7.4418	-0.4185	O	2.8610	7.1033	-1.7382
H	15.8049	7.3512	0.5160	O	3.7675	6.9564	0.2959
S	9.9535	9.0417	5.5384	O	4.3475	7.4701	-3.7870
N	14.4846	3.6204	5.9911	H	3.6604	7.2158	-3.3769
N	12.2876	5.7580	3.1975	C	2.1413	3.8813	-0.4937
N	10.9727	7.8184	5.2874	C	2.5233	2.5073	-0.8054
N	9.9542	9.1180	7.1387	C	2.2285	1.9236	-2.0515
C	13.7352	4.4832	5.9035	C	2.6137	0.6174	-2.3189
C	12.8126	5.5364	5.6872	H	2.4263	0.2177	-3.1606
C	12.4844	5.6994	4.3218	C	3.2730	-0.0828	-1.3366
C	12.2653	6.3138	6.7186	C	3.5704	0.4423	-0.0981
C	11.3641	7.4006	6.4976	H	4.0234	-0.0730	0.5585
C	10.7765	8.1642	7.5714	C	3.1924	1.7349	0.1518
S	13.3699	5.2053	10.1374	H	3.3889	2.1181	0.9992
N	8.8388	10.6266	9.6847	C	3.8597	7.2065	-0.9320
N	11.0357	8.4890	12.4782	C	5.1383	7.6516	-1.4986
N	12.3507	6.4286	10.3883	C	5.3205	7.7821	-2.8908
N	13.3692	5.1290	8.5370	C	6.5182	8.2413	-3.3998
C	9.5882	9.7638	9.7723	H	6.6414	8.3380	-4.3367
C	10.5108	8.7106	9.9886	C	7.5266	8.5551	-2.5229
C	10.8390	8.5476	11.3540	C	7.4097	8.3992	-1.1509
C	11.0580	7.9332	8.9571	H	8.1350	8.6009	-0.5712
C	11.9593	6.8464	9.1782	C	6.2178	7.9472	-0.6579
C	12.5469	6.0828	8.1044	H	6.1187	7.8312	0.2798

Table S9.Calculated total energies and $\langle \widehat{S}^2 \rangle$ values of the four charge–spin states.

	Neutral state				CT state			
	Antiferromagnetic state		Ferrimagnetic state		Ferrimagnetic state		Ferrimagnetic state	
Models	Energy / a.u.	Energy / a.u.	Energy / a.u.	Energy / a.u.	Energy / a.u.	$\langle \widehat{S}^2 \rangle$	Energy / a.u.	$\langle \widehat{S}^2 \rangle$
1-3Ani	–6824.3270	–6824.3234	–6824.3234	–6824.3234	–6824.3234	2.0171	–6824.3271	6.0179
1	–6824.2256	–6824.2282	–6824.2282	–6824.2282	–6824.2282	2.2547	–6824.2270	6.1810

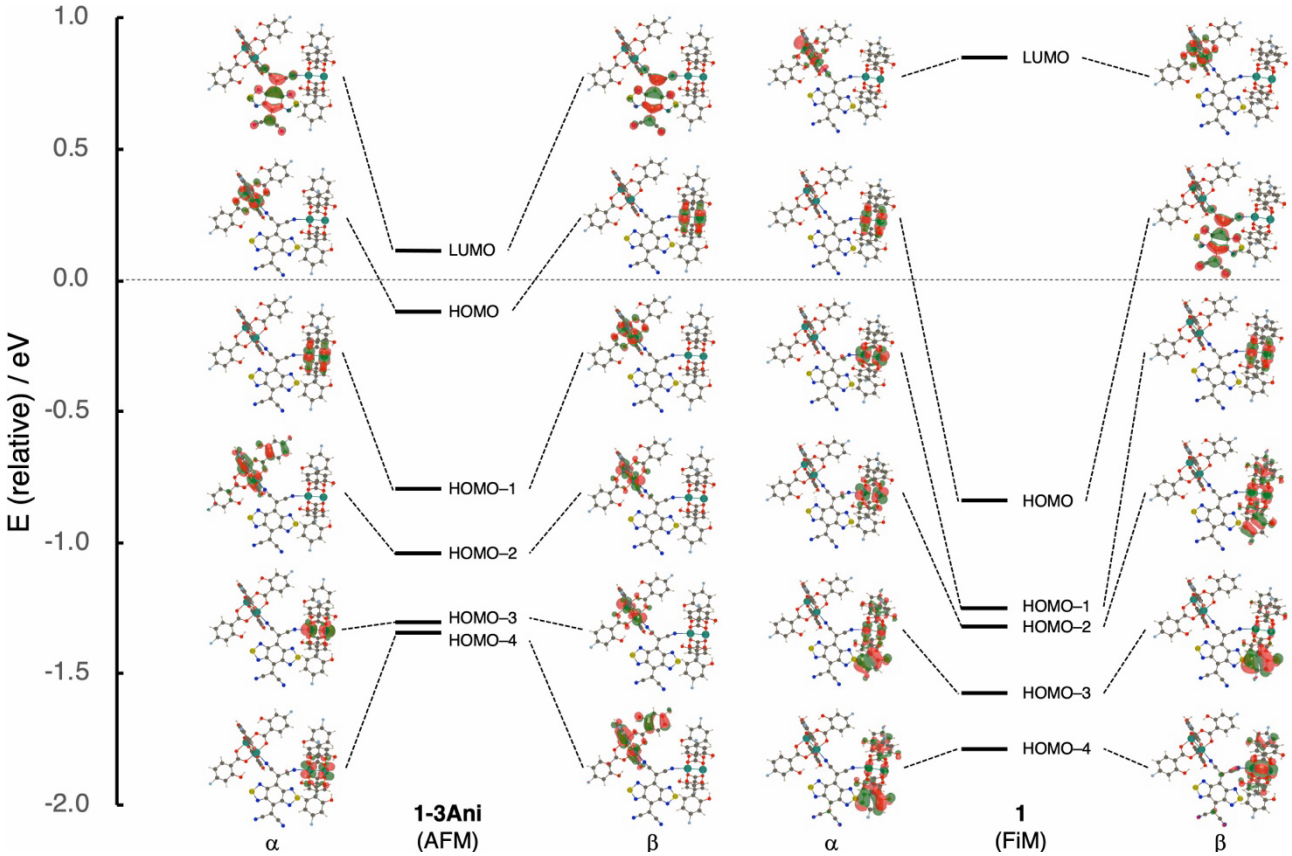

Figure S11. Frontier orbitals from HOMO–4 to LUMO and their relative energy gaps in the **1-3Ani** (AFM) and **1** (FiM) models. The relative α orbital energies are presented here, where the mid-point of the HOMO-LUMO gap is defined as zero.

References in SI

(1) Kistenmacher, T. J.; Emge, T. J.; Bloch, A. N.; Cowan, D. O. Structure of the Red, Semiconducting Form of 4,4′,5,5′-TetramethyI-$\Delta^{2,2'}$-Bi-1,3-Dlselenole-7,7,8,8-Tetracyano-*p*-Quinodimethane, TMTSF-TCNQ. *Acta Cryst.* **1982**, *B38*, 1193-1199.

(2) T. Suzuki, H. Fujii, Y. Yamashita, C. Kabuto, S. Tanaka, M. Harasawa, T. Mukai, T. Miyashi, *J. Am. Chem. Soc.* **1992***, 114, 3034−3043*.

(3) T. Suzuki, C. Kabuto, Y. Yamashita, T. Mukai, T. Miyashi, G. Saito, *Bull. Chem. Soc. Jpn.* **1988***, 61, 483−493*.

(4) Zhang, J.; Kosaka, W.; Sato, H.; Miyasaka, H. Magnet Creation by Guest Insertion into a Paramagnetic Charge-Flexible Layered Metal–Organic Framework. *J. Am. Chem. Soc.* **2021**, *143* (18), *7021–7031*.

(5) Zhang, J.; Kosaka, W.; Liu, Q.; Amamizu, N.; Kitagawa, Y.; Miyasaka, H. CO_2 -Sensitive Porous Magnet: Antiferromagnet Creation from a Paramagnetic Charge-Transfer Layered Metal–Organic Framework. *J. Am. Chem. Soc.* **2023**, *145* (48), *26179–26189*.

(6) Zhang, J.; Kosaka, W.; Kitagawa, Y.; Miyasaka, H. A Metal–Organic Framework That Exhibits CO_2-Induced Transitions between Paramagnetism and Ferrimagnetism. *Nat. Chem.* **2021**, *13* (2), 191–199.

(7) Zhang, J.; Kosaka, W.; Kitagawa, Y.; Miyasaka, H. Host–Guest Hydrogen Bonding Varies the Charge-State Behavior of Magnetic Sponges. *Angew. Chem. Int. Ed.* **2019**, *58* (22), 7351–7356.

(8) Naveen, K.; Reehuis, M.; Adler, P.; Pattison, P.; Hoser, A.; Mandal, T. K.; Arjun, U.; Mukharjee, P. K.; Nath, R.; Felser, C.; Paul, A. K. Reentrant Magnetism at the Borderline between Long-Range Antiferromagnetic Order and Spin-Glass Behavior in the *B*-Site Disordered Perovskite System Ca_{2-x} Sr_xFeRuO_6. *Phys. Rev. B* **2018**, *98* (22), 224423.

(9) Ortega-San Martin, L.; Chapman, J. P.; Lezama, L.; Saiz Garitaonandia, J. J.; Sánchez Marcos, J.; Rodríguez-Fernández, J.; Arriortua, M. I.; Rojo, T. Spin-Glass Behaviour in the Double Perovskite "Sr_2FeTeO_6 " Due to Mis-Site Disorder and Cation Vacancy Formation. *J. Mater. Chem.* **2006**, *16* (1), 66–76.

(10) Gupta, S.; Chakraborty, S.; Pakhira, S.; Biswas, A.; Mudryk, Y.; Kumar, A.; Mukherjee, B.; Okram, G. S.; Das, A.; Pecharsky, V. K.; Mazumdar, C. Experimental Observation of Spin Glass State in the Highly Disordered Quaternary Heusler Alloy FeRuMnGa. *Phys. Rev. B* **2023**, *107* (18), 184408.

(11) Lago, J.; Blundell, S. J.; Eguia, A.; Jansen, M.; Rojo, T. Three-Dimensional Heisenberg Spin-Glass Behavior in $SrFe_{0.90}Co_{0.10}O_{3.0}$. *Phys. Rev. B* **2012**, *86* (6), 064412.

(12) Chakraborty, S.; Gupta, S.; Pakhira, S.; Choudhary, R.; Biswas, A.; Mudryk, Y.; Pecharsky, V. K.; Johnson, D. D.; Mazumdar, C. Ground-State Degeneracy and Complex Magnetism of Geometrically Frustrated $Gd_2Ir_{0.97}Si_{2.97}$. *Phys. Rev. B* **2022**, *106* (22), 224427.